Research Article

Conformable Multifunctional Space Fabric by Metal 3D Printing for Collision Hazard Protection and Self-Powered Monitoring

Yanshuo Sun,[⊥] Chengyu Li,[⊥] Zijie Xu,[⊥] Yaxing Cao, Hengrui Sheng, Zhong Lin Wang,* and Leo N.Y. Cao*

Cite This: https://doi.org/10.1021/acsami.3c15232

Read Online

ACCESS | ☐ Metrics & More | ☐ Article Recommendations | ☐ Supporting Information

ABSTRACT: The monitoring of space debris assumes paramount significance to ensure the sustainability and security of space activities as well as underground bases in outer space. However, designing a wide range monitoring system with easy fabrication, low power, and high precision remains an urgent challenge under the scarcity of materials and extreme environment conditions of outer space. Here, we designed a one-piece, robust, but flexible, and repairable 3D metal-printed triboelectric nanogenerator (FR-TENG) by incorporating the advantages of standardization and customization of outer space 3D metal printing. Inspired by the structure of hexagonal and pangolin scales, a curved structure is ingeniously applied in the design of 3D printed metal to adapt different curved surfaces while maintaining superior compressive strength, providing excellent flexibility and shape adaptability. Benefiting from the unique structural design, the FR-TENG has a minimum length of 1 cm with a weight of only 3.5 g and the minimum weight resolution detected of 9.6 g, with a response time of 20 ms. Furthermore, a multichannel self-powered collision monitoring system has been developed to monitor minor collisions, providing warnings to determine potential impacts on the space station and bases surfaces. The system may contribute to ensuring the successful completion of space missions and providing a safer space environment for the exploration of extraterrestrial life and the establishment of underground protective bases.

KEYWORDS: 3D metal printing, space impact monitoring, triboelectric nanogenerator, self-powered sensing, space debris, wireless sensing

1. INTRODUCTION

The successful launch of the world's first artificial satellite in 1957 symbolized the commencement of human ventures into space. However, the issue of space debris emerged as a significant concern as space exploration progressed, which mainly originates from defunct satellites, discarded rocket stages, and debris generated by accidental collisions and explosions. The extremely high-speed movement and unpredictability pose a potential collision risk to active spacecraft, satellites, space stations, and outer space bases.[1−3] For example, a minor decrease in the air pressure within the International Space Station (ISS) module was observed in 2018, and the astronauts spent several hours searching for the location and cause of the leak, which was mainly attributed to a tiny meteorite impact. Therefore, the monitoring of space debris assumes paramount significance to ensure space and outer space safety as well as the sustainability and security of space activities.[4] Traditional methods for monitoring space debris include ground-based radar, optical observation, and satellite tracking, which have limitations in detecting minor pieces of debris and accurately predicting the trajectories, especially in debris-intensive regions. Moreover, the energy

consumption of sensors poses a critical concern, particularly for spacecraft engaged in prolonged space missions. In the event that a sensor malfunctions or runs out of power, the scarcity of space materials might lead to a critical scenario in which replacement becomes unfeasible. This predicament is particularly pronounced in the unique environment of outer space, owing to the limited availability of resources and the difficulties associated with repairs and replacements. Hence, the development of innovative sensing technologies and advanced monitoring systems to enhance the capabilities of detecting microscopic debris has emerged as an urgent technical challenge for researchers.

Fortunately, the triboelectric nanogenerator (TENG) is an excellent choice based on the coupling of triboelectrification and electrostatic induction first proposed by Wang's group in
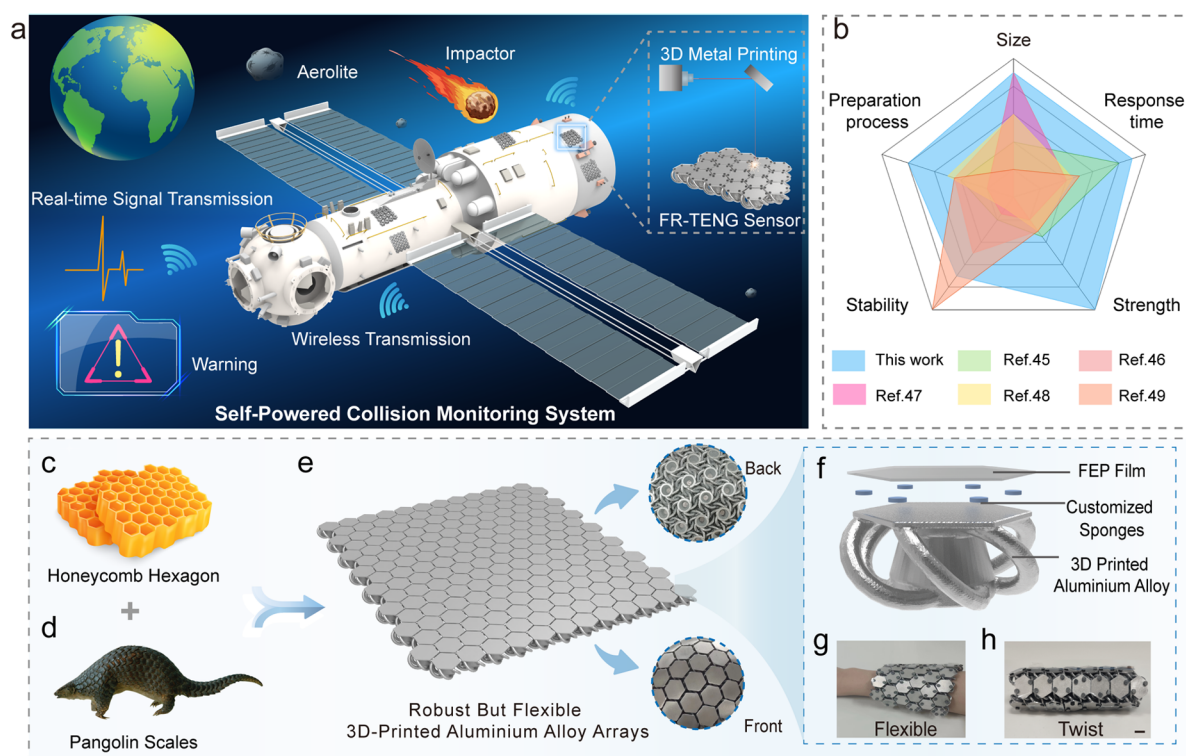
Figure 1. Design and concept of the robust but flexible FR-TENG array inspired by hexagon and pangolin scales. (a) Schematic diagram of SPCMS system. (b) Comparison of FR-TENG with previous studies. (c,d) Schematic diagram of the structures of hexagonal and pangolin scales. (e) 3D printed large-area aluminum alloy arrays; the insets show front and back photographs. (f) The structure of the FR-TENG. (g,h) Photographs of FR-TENG array in different states, and the scale bar is 1 cm.

2012 and is regarded an emerging self-powered sensing technology,[5,6] which has a widespread application in biomedical,[7−9] ocean energy harvesting,[10,11] and self-powered wearable devices.[12,13] The easy and on-site manufacturing and repair of the TENG can be the most valuable feature for outer space applications. First, the TENG boasts unique advantageous features with simple structure, easy fabrication, and high sensitivity in space debris, which easily integrates into the surface of spacecraft or space station to achieve precise monitoring of small impacts, facilitating detection and localization, reducing costs, and enhancing the reliability and stability.[14−17] Second, compared to traditional energy supply methods, TENG converts mechanical energy into electrical energy,[18−20] utilizing electrostatic induction to generate self-powered signals through collisions in space without the need for additional energy supply, thereby eliminating the need for additional energy supply.[21−23] The characteristic bestows the TENG with sustainability and self-sufficiency during prolonged space missions, reducing reliance on external power sources. Furthermore, it is worth pointing out that unlike traditional nonself-powered sensors, the self-powered sensing characteristics of TENG are unable to disrupt the energy distribution and operation of the system in the event of damage, which is critical to the robustness and accuracy of the entire system. In contrast, conventional sensors require a power source and may lead to system interruption when damaged. The self-powered feature of the TENG improves reliability and stability, especially important in space missions, where uninterrupted functionality is critical to mission success and spacecraft safety.

The external management of TENG is another advantageous feature.[24,25] In the pursuit of space missions, the supply of equipment and materials remains a crucial constraint on

human exploration of the depths of the universe. Equipment and structures are susceptible to damage or wear, and reliance on the earth supply undoubtedly leads to increased time and transportation costs. Thus, it is definitely the most promising solution to utilize the equipment and materials available on-site for the preparation of the required supplies and tools. 3D printing technology also known as additive manufacturing (AM) technology, which has a wide range of applications in the medical,[26,27] aerospace,[28,29] and construction fields[30,31] by using metal powders,[32,33] ceramics,[34,35] or polymers[36,37] (perfectly suitable for the wide materials selections of TENG) to prepare simple or complex parts by combining the advantages of standardized and customized production to produce parts with high strength, lightweight, and outstanding mechanical properties.[38−41] Through the innovative prowess of 3D printing, astronauts are bestowed with the power to manufacture essential components, equipment, and replacements in real time, precisely tailored to the unique demands of each mission.[42−44] The remarkable ability eliminates the need for reliance on earth supply, thus streamlining logistics and significantly elevating mission sustainability and reliability. Additionally, 3D printing technology obviates the necessity to premanufacture and package large quantities of equipment instead of manufacturing what is needed on demand in real time. By embracing the advantages of reduced material dependency, customized production, and efficient repair capabilities, 3D printing is a pioneering and transformative solution for space missions, propelling space exploration and sustainable development into new frontiers.

In this study, we present a one-piece, robust but flexible, and repairable 3D metal-printed multifunctional TENG (FR-TENG) for protection, shielding, and impact monitoring on

space station and outer space. The one-piece and on-site manufacturing of 3D printing allows for standardization, customization, and large-scale arrays by fabricating complex devices in a single process, ensuring accuracy and consistency. With a side length of 1 cm and a weight of only 3.5 g, the lightweight design of the TENG unit reduces the weight burden and launch costs of spacecraft, effectively alleviating the difficulty of scarce resources in outer space.

In addition, inspired by the hexagonal and pangolin scale, a curved structure is ingeniously applied in the design of 3D printed FR-TENG to adapt different curved surfaces while maintaining superior compressive strength, providing excellent flexibility and shape adaptability. FR-TENG consists of 3D printed aluminum alloy, fluorinated ethylene propylene (FEP) and customized foam components that enable effortless and precise attachment directly to the surface of the space station or any curved configuration with a minimum weight resolution of only 9.6 g and a response time of 20 ms, permitting the sensing of small weights with high precision and rapidly responding to changes in the external environment.

Furthermore, a multichannel self-powered collision monitoring system (SPCMS) has been developed to monitor small- or large-scale collisions by an array of sensor. The SPCMS system transmits data to a computer in real time and provides alerts to assess potential impacts on the surfaces of the structure, enhancing the operation and protection of the station and enabling digital monitoring. The SPCMS system may play a vital role extending to future explorations of extraterrestrial worlds and the establishment of human underground habitats, providing vital support and assurance for scientific research and space exploration missions.

2. RESULTS AND DISCUSSION

2.1. Concept and Structure of the FR-TENG. At present, traditional space station sensors are facing challenges such as insufficient power supply, low signal and susceptibility to interference, and the requirement for regular replacement and maintenance, leading to increased costs and complexities of space missions. However, the TENG provides a powerful solution for space missions as a sensing technology with the advantages of self-powered, high sensitivity, and durability. Meanwhile, the components used in space station sensors are usually dependent on Earth for supply. It is extremely difficult to maintain and repair components in the event of damage or malfunction, which potentially leads to delays or interruptions in space missions, while space 3D printing technology reduces the dependence on Earth by real-time manufacturing and instant repair on the space station. In addition, light and high-strength metal components are customized according to the specific needs of different missions, effectively improving the mission success and efficiency.

Therefore, in order to solve the above-mentioned problem, a self-powered collision monitoring system (SPCMS) was proposed based on the integration of multifunctional space onsite 3D printing technology and self-powered TENG sensing, enabling signal sensing and sending alarm to the astronauts timely to check the operational status of the space station during collision, as depicted in Figure 1a. Compared with traditional sensors.[45−49] FR-TENG has the structural characteristic of small size, fast response time, high strength and stability, and simple production process as shown in Figure 1b. The superior structural advantages of FR-TENG derive

from the structural characteristic of hexagonal and pangolin scales in nature.

The following sections explain the advantages and details of the design. It is well-known that the hexagon (Figure 1c) demonstrates excellent stability, strength, and easy assembly, while the surface of pangolin scales (Figure 1d) with a hard and layered overlapping structure provides both self-protection and a degree of flexibility. Therefore, we prepared 3D printed FR-TENG by incorporating the advantages of both as depicted in Figure 1e, with the insets showing the front and back photographs. It remains stable under external pressure and impact like the hexagon, rigid but flexible like the scales of pangolin, which can be applied to the curved surface for multiangle monitoring and protection, as illustrated in Figure 1g,h. To further enhance the robustness of the system, the materials need to be investigated in depth.

Here, a systematic exploration of materials, structures, and manufacturing processes was performed. The structural components exposed to external space stations and outer space bases must possess sufficient mechanical properties to withstand harsh space environmental conditions, such as intense radiation, extreme temperatures, and vacuum conditions. Thus, aluminum alloy was chosen as the printing material, which has advantages of light, high strength, and recyclability and is well-suited for utilization in space conditions where materials are scarce. As shown in Figure 1f, each FR-TENG unit consists of only 3D printed aluminum alloy, FEP, and customized foam, providing easy preparation and integration in minutes without sophisticated equipment or complex processes. The top and bottom bases of the aluminum alloy are connected by arcs, and the middle part is a hollow to reduce the overall weight of FR-TENG. Notably, benefiting from the high printing accuracy, customizable production, and lightweight of aluminum alloy material of 3D printing, the customized metal electrodes are small in size (1 cm), light in mass (3.5 g), and flexible as shown in Figures S1. Meanwhile, a 13 cm × 10 cm FR-TENG array weighs only 151 g, demonstrating the excellence and precision of 3D printing.

The combination of 3D and TENG tackles the space sensing: (1) The challenge of supplying sensor components in space is successfully solved, which realizes the large-scale manufacture, replacement, and instant repair of FR-TENG, ensuring the sustainability and stability of the operation for sensors in space. (2) Moreover, 3D printing technology provides material support for the sensing system, realizing efficient material manufacturing and self-powered sensing and offering a viable solution to the problem of scarce material resources in space stations.

2.2. Electrical Output Performance of the FR-TENG. With the unique advantage of self-powered sensing in isolated and remote space environments, the single-electrode TENG eliminates the requirement for an external power source. Besides, its simplified design and the reduction in the number of electrodes provide compatibility with the space station and reduce the possibility of interference from spacecraft materials, ensuring that the overall impact of the system is minimized. Thus, considering the complexity of the space environment and the convenience of easy on-site fabrication and maintenance, a simple structure and easy fabrication of the single-electrode mode FR-TENG was prepared. An FEP film with a high fluorine content was chosen for the friction layer to obtain a high surface charge density, and the working principle is shown in Figure 2a. First, as the FEP contacts the 3D printed

Figure 2. Electrical output performance of the FR-TENG. (a) Working principle of FR-TENG. (b) Simulation results of FR-TENG by COMSOL. (c,d) V_{OC} and I_{SC} of the FR-TENG under different frequencies of 0.5 to 2.5 Hz. (e) Response time of FR-TENG. (f) FR-TENG output performance under different forces of 5 to 50 N. (g) Corresponding force−voltage fitting curves. (h,i) Output performance of FR-TENG under different temperatures (range from 296.15 to 333.15 K) and humidity (range from 25 to 60%). (j) Robustness testing of FR-TENG after 50,000 cycles.

aluminum alloy, a negative frictional charge accumulates on the surface of the FEP while a positive frictional charge is generated on the aluminum surfaces (i). The potential difference between the two surfaces gradually increases during the separation process between FEP and the aluminum alloy, resulting in an instantaneous flow of electrons from the ground

to the aluminum alloy in the external circuit (ii), and the transient flow of electrons continues until the FEP and aluminum alloy are completely separated (iii). Second, the electrons will flow from the aluminum alloy to the ground through the external load as the FEP approaches the aluminum alloy again (iv). The continuous and repetitive contact-
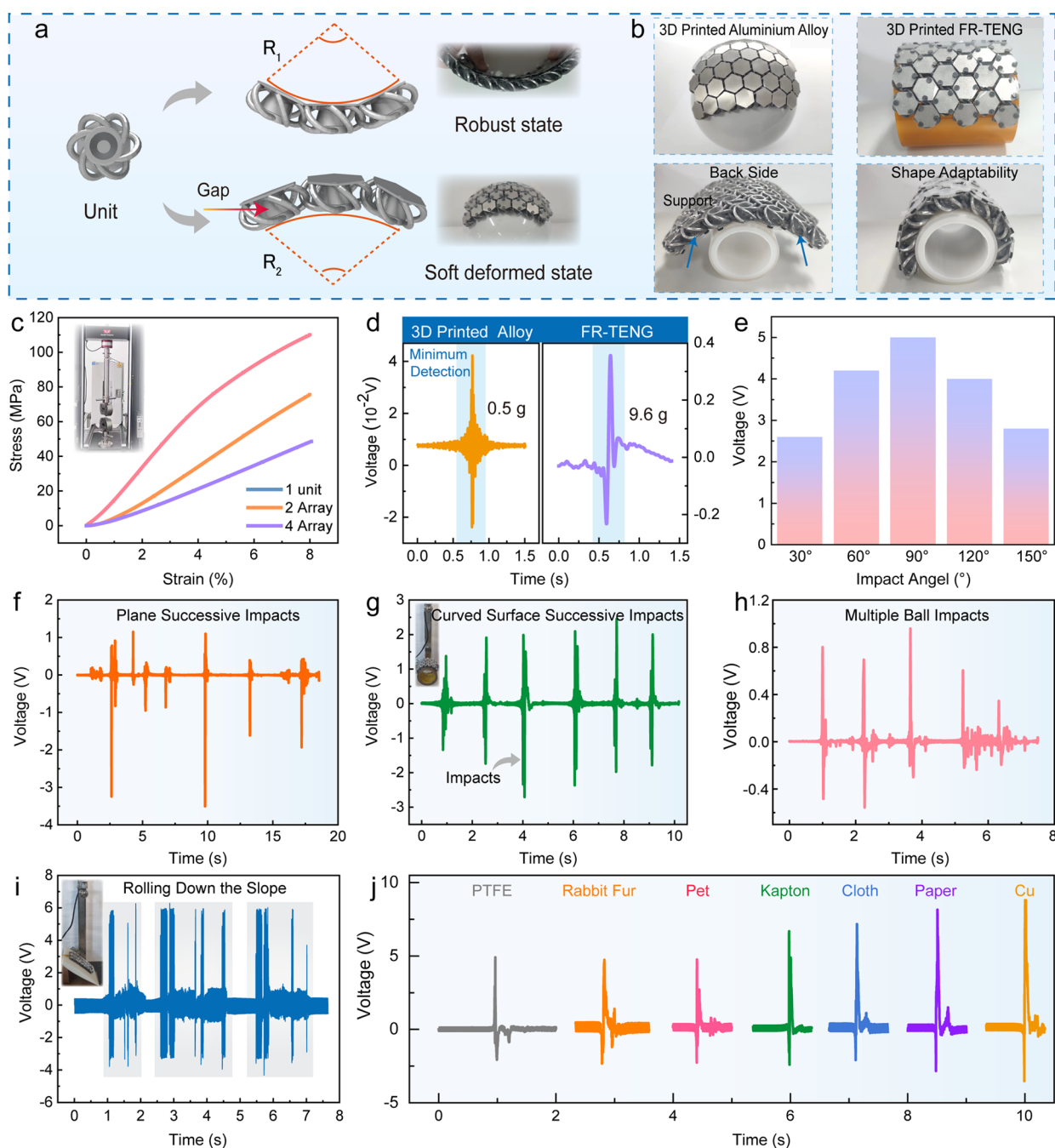
Figure 3. Analysis of the FR-TENG impact signal response. (a) Two states of 3D metal printing FR-TENG. (b) Photographs of FR-TENG and 3D printed aluminum alloy. (c) Stress−strain curves of the aluminum alloys. (d) Minimum weight detection limits for 3D printed aluminum alloys and FR-TENG. (e) FR-TENG impact test at different angles from 30 to 150°. (f,g) The FR-TENG successive impact test on plane and curved surfaces. (h) Electrical signal test of multiple balls impacting FR-TENG continuously. (i) The output performance of the steel ball rolling down from the FR-TENG. (j) Output characteristics of FR-TENG impacts with different materials.

separation of FEP and aluminum alloy generates an alternating current, and the corresponding COMSOL simulation are shown in Figure 2b.

In order to assess the consistency and reliability of TENG in space applications and gain a deeper understanding of its sensitivity and responsiveness for external stimuli, we tested the electrical output performance of the 2 cm × 2 cm FR-TENG under normal environmental conditions. The frequency of contact-separation between the two friction layers of the FR-TENG was gradually increased from 0.5 to 2.5 Hz. The open circuit voltage (Figure 2c) and charge (Figure S2) remained

relatively stable at 4 V/cm^2 and 1.25 nC/cm^2, respectively, while the current gradually increased from 4.5 to 20 nA/cm^2 (Figure 2d). The results are consistent with previous theoretical studies, primarily indicated by the fact that I_{SC} is determined by the contact-separation rate, while V_{OC} and Q_{SC} are mainly influenced by the displacement. Given the same external pressure stimulus, a higher operating frequency reduces the duration of the current, enhancing the charge transfer rate and the I_{SC} amplitude. Moreover, TENG is a self-powered sensing technology that operates without external power sources, and the response time is critical for real-time

monitoring sensing. The fast response time of the FR-TENG of approximately 20 ms is shown in Figure 2e, providing the astronauts a timely warning information. Additionally, investigating the output performance of the TENG at different pressures is essential to ensure its ability to be self-powered in space, which will eliminate the dependence on external power sources, thereby enhancing reliability and stability. The voltage signal gradually increases with increasing applied force in the pressure range of 5−60 N as shown in Figure 2f, and the corresponding linear response of the voltage signal versus force is shown in Figure 2g. The inset displays a schematic of the experimental setup for testing, including the linear motor, force meter, and electrometer. It is mainly attributed to the fact that the applied force increases the contact area between the friction layers during the friction process and the enhanced surface charge density of the material,[50] resulting in improved output performance of the FR-TENG. However, as the surface charge density tends to saturate, the output performance of TENG tends to stabilize.

Space environments exhibit wide temperature and humidity fluctuations, posing challenges, such as thermal expansion, structural distortion, and material degradation, for sensors exposed to drastic temperature shifts. Additionally, humidity conditions possibly affect the electronic components and circuits of sensors adversely through corrosion and oxidation. Thus, it is necessary to perform temperature and humidity testing for the FR-TENG sensors. The results in Figure 2h (temperature range 296.15−333.15 K) and Figure 2i (humidity range 25−60%) indicate the decrease in output voltage with increasing temperature and humidity, which is largely caused by the pyroelectric effect of electrons and the decrease in surface charge density. Figures S3 illustrates the characterization of the surface properties of FR-TENG and changes at different temperatures and humidities. The Trek electrostatic voltmeter was used to automatically scan the surface potential of the plates from top to bottom and from left to right in the prefriction and after-friction tests on the FEP material. It can be seen from the graph that the potential is very small before friction and increases after friction, demonstrating the excellent electrical effect of TENG. Furthermore, although only tested up to 333.15 K, the TENG can withstand temperatures as high as 573 K according to relevant literature,[51−54] promising potential applications in fields such as space monitoring and extreme environments. In addition, space as a strong radiation environment may affect the material properties, electron transport, and stability of TENG. Tang et al.[55] investigated the surface modification of dielectric materials induced by γ-rays and studied the effect on contact initiation. It was demonstrated that the high energy of γ-rays breaks and rearranges certain chemical bonds in the polymers, thus altering the electron density and enhancing the electron transfer capability of the dielectric material, proving the application of TENG for the fabrication of materials with high resistance to radiation and sensing in space or other high-radiation environments.

Furthermore, the charging of different capacitors by FR-TENG at a frequency of 2.5 Hz is illustrated in Figure S2. It can be observed that the charging rate decreases with increasing capacitance for the same charging time, and a higher voltage may be obtained by charging with a smaller capacitor. Similarly, the arrangement of units increases the contact area, which enhances charge transfer and improved feasibility of TENG in supplying environmentally friendly, self-

sustaining power sources for small electronic devices. As depicted in Figure S4, the voltage gradually increases from 5 to 35 V as the area increases, which is attributed to the fact that the charge transfer between the friction layers increases with the contact area. With space missions typically endure for extended periods, sensors require long-term durability to operate continuously and stable in space environments without damage or malfunction. Therefore, the robustness of FR-TENG was tested at a frequency of 2.5 Hz. The output voltage of FR-TENG remains stable after 50,000 cycles of continuous operation without a significant drop as shown in Figure 2j, and the inset shows a zoomed-in graph of the data, which demonstrates the superior stability and robustness.

2.3. 3D Metal Printing and Sensor Parameters. Metal 3D printing technology meets the requirements of material scarcity, customization, one-piece, and high-temperature resistance in the space environment, providing a more reliable solution for component manufacturing in space missions. This technology has revolutionized the production of robust custom metal components, addressing the challenges posed by limited materials and the unique demands of space exploration. Metal powders are machined layer by layer to solid parts by employing techniques such as selective laser melting or electron beam melting, as shown in the schematic diagram of Figure S5, which enables the realization of sophisticated structures and customized designs. 3D printing technology allows strong but relatively lightweight metal parts compared with other techniques, thus finding extensive applications in the aerospace, medical, and automotive industries. Moreover, one-piece molding achieved customized designs and light-weight components without the need for additional assembly, thus reducing the risk of part failure and structural damage in extreme environments. For instance, the one-piece 3D printed aluminum alloy array exhibits excellent toughness and flexibility, as shown in Figure 3a. First, benefiting from the unique structural design, the interconnection of each unit and the curved structure enable the formation of large gaps between the units that enhance flexibility and shape adaptability. According to the radius of curvature formula[56,57] (eq 1), the upward bending radius of curvature R_1 of FR-TENG is 7.5 cm with a curvature of 13.3 m^{-1}, while the downward bending radius of curvature R_2 is 1.2 cm, with a curvature of 83.3 m^{-1}.

$$K = \frac{1}{R} \tag{1}$$

Here, K is the curvature and R is the radius. The extremely low radius of curvature allows FR-TENG to adapt to different curved surfaces (cylindrical, circular, and shaped), as described in Figure 3b and Figure S6. Furthermore, the deformable structure also exhibits robustness when subjected to reverse stress on the backside. Aluminum alloys typically possess high compressive strength in conventional manufacturing process. A single aluminum unit withstands a stress of 110 MPa, while an array of four aluminum alloy units is subjected to less stress at the same compression strain than a single unit aluminum alloy, as shown in the stress−strain relationship diagram (Figure 3c). It is primarily attributed to the increased area of the array, which reduces the interaction between adjacent units and enables the units to jointly withstand external pressures, thereby reducing the stress on each unit and enhancing the overall cushioning capacity of the array. Thus, 3D printed metal has characteristics that distinguish it from traditional soft
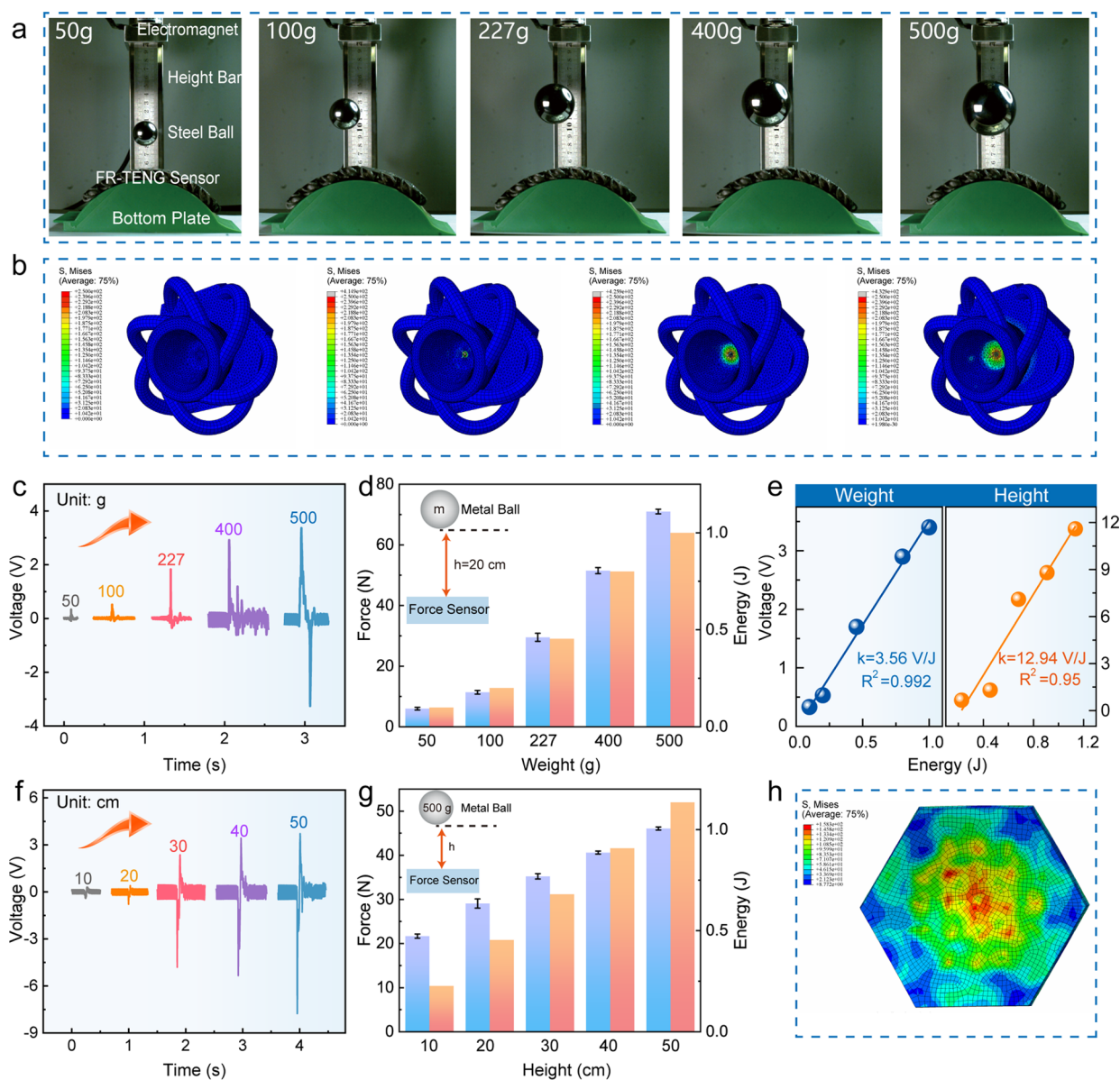
Figure 4. Analyzing collision signals and sensing characteristics. (a) Photographs of steel balls with different weights falling at the same height. (b) Stress cloud distribution of FR-TENG subjected to ball impact simulated by Abaqus software. (c) Voltage signals under different weights with the same height. (d) Corresponding force and gravitational potential energy at different weights. (e) Linear fitting curves of FR-TENG at different weights and heights. (f) Voltage signals under different heights with the same weight. (g) Corresponding force and gravitational potential energy at different heights. (h) Stress simulation cloud for ball drop by Abaqus software.

TENG with advantages of better compression strength, robustness, stability, offering potential applications in the fields of smart security, aerospace, and energy. High sensitivity is another significant advantage of TENG. In space, small collisions and temperature changes may have an impact on the operational status of the space station. While FR-TENG is able to convert small changes into electrical signals with a minimum weight resolution of 9.6 g, pure 3D printed aluminum alloys detect weight as low as 0.5 g, as shown in Figure 3d. The high sensitivity and low detection resolution of FR-TENG provide real-time monitoring and feedback to the space station, supporting the stability and safety of the station. The FR-TENG also performs well with different impact angles, as shown in Figure 3e, where the sensor still has a stable voltage output when changing the impact angle (30−150° in 30° steps).

Benefiting from the design of the curved structure, 3D printing technology enables the FR-TENG to flexibly adapt to different curved shapes. Thus, the steel ball was controlled to impact the FR-TENG continuously in plane, curved surfaces, and multiple balls by controlling steel balls through the ball drop experimental machine, which proved that FR-TENG is able to generate stable electric signals under continuous impact (Figure 3f−h). In addition, FR-TENG generates stable electrical signals as the ball rolls down as shown in Figure 3i, which greatly broadens the application range of FR-TENG. Furthermore, extensive research was conducted by subjecting the FR-TENG to impacts from various commonly available materials to test the response outputs, revealing the wide applicability of the TENG in a variety of applications. The versatility of TENG materials is evident to generate signals upon impact from a variety of materials (PTFE, rabbit fur,
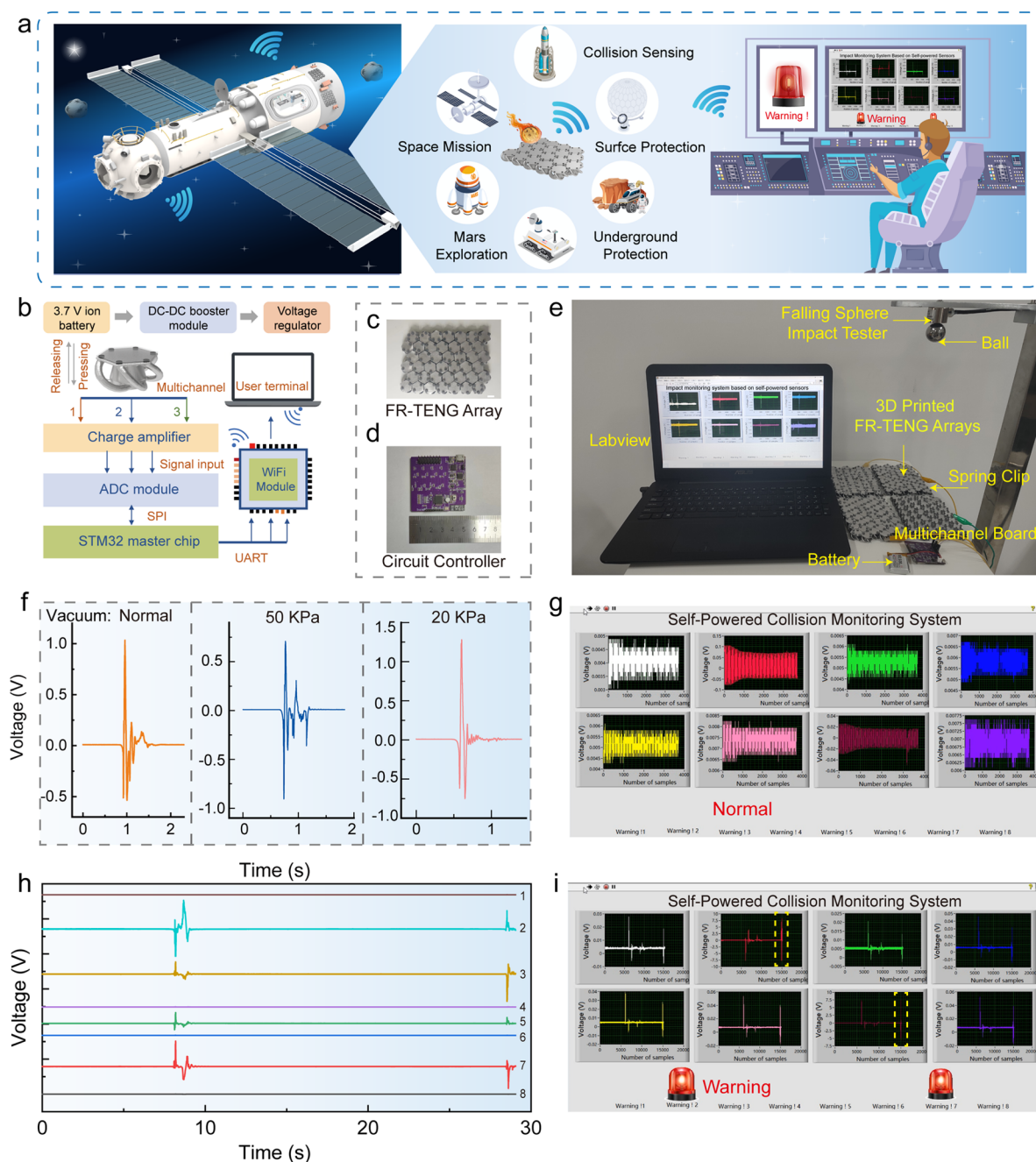
Figure 5. Multichannel wireless impact monitoring system in real time. (a) Schematic diagram of the FR-TENG based self-powered collision monitoring system and potential applications. (b) Multichannel circuit acquisition system workflow diagram and components. (c) Photographs of FR-TENG array with a scale of 1 cm. (d) Photographs of circuit controller. (e) Photographs of multichannel impact monitoring system tests. (f) The output performance of ball impact FR-TENG at different vacuum levels. (g) Screenshot of the user interface of the SPCMS system under normal conditions. (h) The test when four balls impact the multichannel system. (i) Screenshot of the LabVIEW system with the SPCMS system in the impact state.

PET, Kapton, cloth, paper, and Cu) as shown in Figure 3j, which highlights the broad applicability and adaptability of TENG based self-powered sensing.

2.4. Analyzing Collision Signals and Sensing Characteristics. In order to further simulate the protective features as well as the energy harvesting characteristics of the FR-TENG, a drop hammer test system including a force sensor and a high-speed camera was employed to load the impact excitation. The force sensor was used to record and collect the impact force after the collision, the high-speed camera was used to capture the subtle changes, and the magnitude of the impact force of

which was changed by controlling the height and weight. The impact sensitivity characteristics of FR-TENG at different weights (50−500 g) as well as different heights captured by a high-speed camera are shown in Figure 4a and Figure S7. It was observed from the figure that the rebound height and velocity increased gradually with the increase in weight and height. The response of the FR-TENG-based impact was obtained by the form of voltage signals, and the voltage signals increased gradually with the increase of the weight by releasing the steel balls with different weights (50, 100, 227, 400, and 500 g) at the same height as shown in Figure 4c, which

resulted in a higher voltage output for a higher drop distance. In addition, both impact force and gravitational potential energy exhibit continuous increments with increasing steel ball weight according to the gravitational potential energy eq 2 and force sensor (Figure 4d), displaying a favorable linear response, and the inset shows a schematic diagram of the ball drop with different weights.

$$E = mgh \tag{2}$$

where E is the gravitational potential energy, m is the mass, g is the gravitational acceleration of Earth's surface, and h is the height of fall. Similarly, the impact characteristics of a steel ball of the same weight dropped from different heights (10, 20, 30, 40, and 50 cm) were also tested. It can be seen from the figures that the voltage signal increases gradually with increasing height (Figure 4f), the gravitational potential energy and the impact force also increase as well (Figure 4g), and the inset shows the schematic diagram of a ball of the same weight dropped at different heights. In addition, the linear fit of FR-TENG at different heights, weights, and energies is shown in Figure 4e, and both exhibited excellent linear response. It was demonstrated that the output voltage and impact energy of the TENG-based impact sensor depend on the corresponding height and weight, and the result was also consistent with theory:

$$\text{work done} = \frac{1}{2}mv_1^2 - \frac{1}{2}mv_0^2 \tag{3}$$

where m is the weight of the metal ball, V_0 is the initial velocity equal to zero, V_1 is the velocity of the rebound, d is the distance covered from the impact, g is the gravitational acceleration, and h is the height of descent. Thus, the impact force is determined by the following formula:

$$F_{\text{impact}} = \frac{\text{work done}}{d} = \frac{\frac{1}{2}mv_1^2}{d} = \frac{mgh}{d} \tag{4}$$

Owing to almost the same value of d, thus the impact force is related to weight and height, proving the extremely high reliability and accuracy of the TENG sensor in measuring and handling objects of different heights or weights. The stress cloud of the FR-TENG sensor during the impact of a 500 g steel ball is illustrated in Figure 4h. It can be seen from the figure that the impact point in the center suffers the highest stress and spreads to the surrounding area with uniform force, which indicates that the hexagonal shape is able to withstand the external stresses more uniformly and improves the strength and stability of the structure.

In addition, in order to realistically understand the impact situation in space, we simulated the impact of a ball with a diameter of 0.4 mm, a weight of 0.08 g, and a collision velocity of 5 km/s on the FR-TENG sensor by Abaqus software, and the simulation results are shown in Figure 4b, with the stress values reacted by the colors. It is known from the figure that the impact point is subjected to the maximum stress during the process of impact, and the stress value spreads from the center to the surrounding and gradually decreases. Despite the high strength of the 3D printed metal, FR-TENG still suffers breakage under the impact of high-speed motion in space. However, the remaining parts are subjected to relatively less stress and deformation except for the center breakage region, proving the unique advantage of TENG that the partial breakage unable affect the operation of the whole device, and

the remaining part is still capable of self-powered sensing. These findings not only provide robust support for our research but also offer fresh insights and directions for designing and implementing devices in space environments.

2.5. Multichannel Self-Powered Wireless Impact Monitoring System. The unique combination of robustness and flexibility of FR-TENG enables direct integration on the surface of the space station without additional burdens and operational complexity in the complex environment of space. The design feature not only enables multiangle monitoring and sensing but also provides an efficient and reliable monitoring and sensing solution for the space station. Therefore, to demonstrate the practical application of FR-TENG as a self-powered sensor, we show a multichannel wireless collision signal monitoring system based on FR-TENG self-powered sensors as shown in Figure 5a. The system mainly consists of FR-TENG arrays, signal control circuits, and the LabVIEW system to achieve impact monitoring and emergency alarm features based on voltage signals generated by impacts. Meanwhile, the circuit part mainly consists of WIFI module, analog-to-digital (AD) acquisition module, and charge amplifier controlled by STM32 to achieve wireless communication of sensing signals as displayed in Figure 5b and Figure S9a, with multichannel signal acquisition and processing to achieve long-distance transmission and real-time impact alerts through WIFI transmission and signal control. Figure 5c,d shows the relevant photographs of the FR-TENG sensor arrays and the STM32 board; each FR-TENG array measures 10 cm × 13 cm and connected with a separate channel. For instance, FR-TENG immediately generates an output signal and transmits to the LabVIEW of the computer for alarming when an object impacts the surface of the sensor array. The real-time output and processing of signals demonstrate the superior performance of FR-TENG as a self-powered sensing technology, realizing the monitoring and alarming of space station safety without relying on external power sources.

In addition, the output performance of FR-TENG sensors in different vacuum environments was extensively tested to explore its applicability in the space environment. The FR-TENG sensor produces a stable voltage signal under both normal atmospheric conditions, and different vacuum degrees (50 and 20 KPa) are shown in Figure 5f, which provides strong support for its application in space. Multichannel data acquisition systems enable real-time monitoring and recording of multiple impact events, thus providing a more comprehensive assessment of the occurrence and effects of collisions. It is critical for ensuring the safety and structural health of space station, as impacts at different locations may affect different parts of the station to different degree. A schematic of the multichannel test system is shown in Figure 5e, where the distance and weight of the dropped balls are controlled by the ball drop tester. Figure 5h demonstrates the simultaneous impacts on four channels, and Figure S9b and Video S1 (Supporting Information) demonstrate single-channel crash sensing, where the system generates an early warning in the event of a collision. Meanwhile, the system operation under normal and impact conditions is illustrated in Figure 5g–i and Figure S10. In normal conditions, the interface displays the baseline signal, and different signals were generated simultaneously when the two balls dropped onto the FR-TENG array as displayed in Video S2 (Supporting Informaton), providing intuitive visualization of data and alarm information, which enables the astronauts to quickly obtain information about the

impact event and respond in time. The advantages of standardized and customized space 3D printing technology combined with TENG self-powered sensing will play an important role in long-term deep space exploration, protection and autonomous manufacturing for space missions to support the maintenance and restoration of the space station.

■ CONCLUSIONS

In summary, we designed a one-piece, robust, but flexible 3D metal-printed FR-TENG inspired by the structure of hexagons and pangolin scales to achieve large-scale fabrication by combining the advantages of 3D printing standardization and customization. Benefiting from the unique curved structural design, FR-TENG arrays exhibit flexibility and shape adaptability to adapt to any curved surface as well as maintain high strength. The FR-TENG sensor had a minimum unit size of only 1 cm and a weight of 3.5 g and a minimum weight resolution of only 9.6 g with a response time of 20 ms. In addition, a multichannel SPCMS system was developed based on self-powered sensing to monitor small-scale collisions and transmit the data in real time to a computer to provide an early warning for astronauts. Meanwhile, the LabVIEW interface also features data logging and storage functions to save historical data for subsequent analysis and evaluation. With such a user interface, astronauts monitor and recognize anomalous events in real time and take necessary measures to guarantee the safety and operation of the space station. Furthermore, the SPCMS system is critical for monitoring extraterrestrial life, surface features, and safety measures on alien planets, playing a vital role that extends to future explorations of extraterrestrial worlds and the establishment of human underground habitats, providing vital support and assurance for scientific research and space exploration missions.

4. EXPERIMENTAL SECTION

4.1. Fabrication of FR-TENG. The preparation of FR-TENG is very simple and consists of only two to three components. First, the aluminum alloy array was printed by a mature sophisticated Farsoon Technologies SS 316L metal printer, and then the FR-TENG was assembled by sequentially attaching custom-made foams and adhesive 22 μm FEP films in a process that took only a few minutes; thus, the FR-TENG sensor was prepared and completed.

4.2. Software and Simulation. LabVIEW 2018 and Origin 2018 were used to process and calculate the data, and COMSOL Multiphysics 5.4 was used to simulate the contact separation process of FR-TENG by the finite element method. Abaqus was used to simulate the analysis of forces on a falling ball.

4.3. Characterization and Measurement. A linear motor (Linmot E1100) was used to drive the FR-TENG device during measurements. The open-circuit voltage and short-circuit current and charge were measured with a programmable electrometer (Keithley, model 6514). The software platform adopted LabVIEW to realize real-time data acquisition. The compression performance of the FR-TENG array was tested by means of an experimental compressor, comprising a power management module, a 16-bit AD acquisition module, a preamplifier, an ESP32 WIFI module, and an STM32L431 main control chip. The front-end amplifier amplifies the signal and sends it to the AD chip for digital processing and then sends it to the data terminal through the WIFI module under the control of the main control chip. The terminal uses the LabVIEW computer program to receive, display, and store data. Aluminum arrays were printed on sophisticated state-of-the-art Farsoon Technologies SS 316L metal printers, and stress compression was tested by an Instron universal testing machine.

■ ASSOCIATED CONTENT

Data Availability Statement

The data that support the findings of this study are available from the corresponding author upon reasonable request.

Ⓢ Supporting Information

The Supporting Information is available free of charge at https://pubs.acs.org/doi/10.1021/acsami.3c15232.

Supporting Information is available from the authors. Pictures of FR-TENG in terms of size, weight and flexibility (Figure S1); The electrical properties of FR-TENG (Figure S2); Characterization of the surface properties of FR-TENG and changes at different temperatures and humidities (Figure S3); Output performance of FR-TENG with different areas (Figure S4); Schematic diagram of the 3D printing metal process (Figure S5); The bending photograph of FR-TENG and the stresses in different aluminum alloy arrays (Figure S6); Specific parameters and devices for steel ball impacts FR-TENG (Figure S7); Simulating space impact of FR-TENG (Figure S8); Multichannel testing of FR-TENG (Figure S9); Multichannel application demonstration diagram (Figure S10) (PDF)

Single-channel impact based on a multichannel self-powered collision monitoring system (Video S1) (MP4)

Two-channel impact based on a multichannel self-powered collision monitoring system (Video S2) (MP4)

■ AUTHOR INFORMATION

Corresponding Authors

Zhong Lin Wang − *Beijing Institute of Nanoenergy and Nanosystems, Chinese Academy of Sciences, Beijing 101400, P. R. China; School of Nanoscience and Engineering, University of Chinese Academy of Sciences, Beijing 100049, P. R. China; School of Materials Science and Engineering, Georgia Institute of Technology, Atlanta, Georgia 30332-0245, United States;* ⓞ orcid.org/0000-0002-5530-0380; Email: zhong.wang@mse.gatech.edu

Leo N.Y. Cao − *Beijing Institute of Nanoenergy and Nanosystems, Chinese Academy of Sciences, Beijing 101400, P. R. China; School of Nanoscience and Engineering, University of Chinese Academy of Sciences, Beijing 100049, P. R. China;* ⓞ orcid.org/0000-0002-2027-2631; Email: caonanying@binn.cas.cn

Authors

Yanshuo Sun − *Beijing Institute of Nanoenergy and Nanosystems, Chinese Academy of Sciences, Beijing 101400, P. R. China; School of Nanoscience and Engineering, University of Chinese Academy of Sciences, Beijing 100049, P. R. China*

Chengyu Li − *Beijing Institute of Nanoenergy and Nanosystems, Chinese Academy of Sciences, Beijing 101400, P. R. China; School of Nanoscience and Engineering, University of Chinese Academy of Sciences, Beijing 100049, P. R. China*

Zijie Xu − *Beijing Institute of Nanoenergy and Nanosystems, Chinese Academy of Sciences, Beijing 101400, P. R. China; School of Nanoscience and Engineering, University of Chinese Academy of Sciences, Beijing 100049, P. R. China*

Yaxing Cao − *Beijing Institute of Nanoenergy and Nanosystems, Chinese Academy of Sciences, Beijing 101400, P. R. China; School of Nanoscience and Engineering,*

University of Chinese Academy of Sciences, Beijing 100049, P. R. China

Hengrui Sheng − Beijing Institute of Nanoenergy and Nanosystems, Chinese Academy of Sciences, Beijing 101400, P. R. China; Center on Nanoenergy Research, School of Physical Science and Technology, Guangxi University, Nanning 530004, P.R. China

Complete contact information is available at:
https://pubs.acs.org/10.1021/acsami.3c15232

Author Contributions
⊥Y.S., C.L., and Z.X. contributed equally to this work.

Notes
The authors declare no competing financial interest.

■ ACKNOWLEDGMENTS

■ REFERENCES

(1) Loomis, I. NASA Sensor to Study Space Junk the Size of Dust. *Science* **2017**, *358* (6368), 1234−1234.

(2) Crowther, R. Space Junk-Protecting Space for Future Generations. *Science* **2002**, *296* (5571), 1241−1243.

(3) Krag, H. A Sustainable Use of Space. *Science* **2021**, *373* (6552), 259−259.

(4) Loomis, I. Air Force Turns a Keen Eye on Space Junk. *Science* **2015**, *347* (6218), 115−115.

(5) Fan, F. R.; Tian, Z. Q.; Lin Wang, Z. Flexible Triboelectric Generator. *Nano Energy* **2012**, *1* (2), 328−334.

(6) Fan, F.; Lin, L.; Zhu, G.; Wu, W.; Zhang, R.; Wang, Z. L. Transparent Triboelectric Nanogenerators and Self-Powered Pressure Sensors Based on Micropatterned Plastic Films. *Nano Lett.* **2012**, *12* (6), 3109−3114.

(7) Hinchet, R.; Yoon, H.-J.; Ryu, H.; Kim, M.-K.; Choi, E.-K.; Kim, D.-S.; Kim, S.-W. Transcutaneous Ultrasound Energy Harvesting Using Capacitive Triboelectric Technology. *Science* **2019**, *365* (6452), 491−494.

(8) Lee, D. M.; Rubab, N.; Hyun, I.; Kang, W.; Kim, Y. J.; Kang, M.; Choi, B. O.; Kim, S. W. Ultrasound-Mediated Triboelectric Nanogenerator for Powering on-Demand Transient Electronics. *Sci. Adv.* **2022**, *8* (1), eabl8423−eabl8430.

(9) Han, S. A.; Seung, W.; Kim, J. H.; Kim, S.-W. Ultrathin Noncontact-Mode Triboelectric Nanogenerator Triggered by Giant Dielectric Material Adaption. *ACS Energy Lett.* **2021**, *6* (4), 1189−1197.

(10) Zhai, H.; Ding, S.; Chen, X.; Wu, Y.; Lin Wang, Z. Advances in Solid−Solid Contacting Triboelectric Nanogenerator for Ocean Energy Harvesting. *Mater. Today* **2023**, *65*, 166−188.

(11) Zhu, C.; Wu, M.; Liu, C.; Xiang, C.; Xu, R.; Yang, H.; Wang, Z.; Wang, Z.; Xu, P.; Xing, F.; Wang, H.; Xu, M. Highly Integrated Triboelectric-Electromagnetic Wave Energy Harvester toward Self-Powered Marine Buoy. *Adv. Energy Mater.* **2023**, *13* (37), 2301665−2301675.

(12) Shi, Y.; Yang, P.; Lei, R.; Liu, Z.; Dong, X.; Tao, X.; Chu, X.; Wang, Z. L.; Chen, X. Eye Tracking and Eye Expression Decoding Based on Transparent, Flexible and Ultra-Persistent Electrostatic Interface. *Nat. Commun.* **2023**, *14* (1), 3315−3326.

(13) Lu, Y.; Tian, H.; Cheng, J.; Zhu, F.; Liu, B.; Wei, S.; Ji, L.; Wang, Z. L. Decoding Lip Language Using Triboelectric Sensors with Deep Learning. *Nat. Commun.* **2022**, *13* (1), 1401−1412.

(14) Li, C.; Xu, Z.; Xu, S.; Wang, T.; Zhou, S.; Sun, Z.; Wang, Z. L.; Tang, W. Miniaturized Retractable Thin-Film Sensor for Wearable Multifunctional Respiratory Monitoring. *Nano Res.* **2023**, *16* (9), 11846−11854.

(15) Xu, Z.; Cao, L. N. Y.; Li, C.; Luo, Y.; Su, E.; Wang, W.; Tang, W.; Yao, Z.; Wang, Z. L. Digital Mapping of Surface Turbulence Status and Aerodynamic Stall on Wings of a Flying Aircraft. *Nat. Commun.* **2023**, *14* (1), 2792−2802.

(16) Hu, S.; Yuan, Z.; Li, R.; Cao, Z.; Zhou, H.; Wu, Z.; Wang, Z. L. Vibration-Driven Triboelectric Nanogenerator for Vibration Attenuation and Condition Monitoring for Transmission Lines. *Nano Lett.* **2022**, *22* (13), 5584−5591.

(17) Li, C.; Liu, D.; Xu, C.; Wang, Z.; Shu, S.; Sun, Z.; Tang, W.; Wang, Z. L. Sensing of Joint and Spinal Bending or Stretching Via a Retractable and Wearable Badge Reel. *Nat. Commun.* **2021**, *12* (1), 2950−2960.

(18) Cao, Y.; Su, E.; Sun, Y.; Wang, Z. L.; Cao, L. N. Y. A Rolling-Bead Triboelectric Nanogenerator for Harvesting Omnidirectional Wind-Induced Energy toward Shelter Forests Monitoring. *Small* **2023**, 2307119−2307128.

(19) Su, E.; Li, H.; Zhang, J.; Xu, Z.; Chen, B.; Cao, L. N. Y.; Wang, Z. L. Rationally Designed Anti-Glare Panel Arrays as Highway Wind Energy Harvester. *Adv. Funct. Mater.* **2023**, *33* (17), 2214934−2214943.

(20) Cao, L. N. Y.; Xu, Z.; Wang, Z. L. Application of Triboelectric Nanogenerator in Fluid Dynamics Sensing: Past and Future. *Nanomaterials (Basel)* **2022**, *12* (19), 3261−3284.

(21) Deng, Z.; Xu, L.; Qin, H.; Li, X.; Duan, J.; Hou, B.; Wang, Z. L. Rationally Structured Triboelectric Nanogenerator Arrays for Harvesting Water-Current Energy and Self-Powered Sensing. *Adv. Mater.* **2022**, *34* (39), 2205064−2205072.

(22) Zhan, F.; Wang, A.; Xu, L.; Lin, S.; Shao, J.; Chen, X.; Wang, Z. L. Electron Transfer as a Liquid Droplet Contacting a Polymer Surface. *ACS Nano* **2020**, *14* (12), 17565−17573.

(23) Zhao, H.; Xu, M.; Shu, M.; An, J.; Ding, W.; Liu, X.; Wang, S.; Zhao, C.; Yu, H.; Wang, H.; Wang, C.; Fu, X.; Pan, X.; Xie, G.; Wang, Z. L. Underwater Wireless Communication Via TENG-Generated Maxwell's Displacement Current. *Nat. Commun.* **2022**, *13* (1), 3325−3334.

(24) Zhang, C.; Chen, J.; Xuan, W.; Huang, S.; You, B.; Li, W.; Sun, L.; Jin, H.; Wang, X.; Dong, S.; Luo, J.; Flewitt, A. J.; Wang, Z. L. Conjunction of Triboelectric Nanogenerator with Induction Coils as Wireless Power Sources and Self-Powered Wireless Sensors. *Nat. Commun.* **2020**, *11* (1), 58−67.

(25) Yu, X.; Fu, S.; Zuo, X.; Zeng, J.; Shan, C.; He, W.; Li, W.; Hu, C. Moisture Resistant and Stable Wireless Wind Speed Sensing System Based on Triboelectric Nanogenerator with Charge-Excitation Strategy. *Adv. Funct. Mater.* **2022**, *32* (44), 2207498−2207506.

(26) Alizadehgiashi, M.; Nemr, C. R.; Chekini, M.; Pinto Ramos, D.; Mittal, N.; Ahmed, S. U.; Khuu, N.; Kelley, S. O.; Kumacheva, E. Multifunctional 3D-Printed Wound Dressings. *ACS Nano* **2021**, *15* (7), 12375−12387.

(27) Joung, D.; Lavoie, N. S.; Guo, S.; Park, S. H.; Parr, A. M.; McAlpine, M. C. 3D Printed Neural Regeneration Devices. *Adv. Funct. Mater.* **2019**, *30* (1), 1906237−1906261.

(28) Murr, L. Frontiers of 3D Printing/Additive Manufacturing: From Human Organs to Aircraft Fabrication. *J. Mater. Sci. Technol.* **2016**, *32* (10), 987−995.

(29) Ngo, T.; Kashani, A.; Imbalzano, G.; Nguyen, K.; Hui, D. Additive Manufacturing (3D Printing): A Review of Materials, Methods, Applications and Challenges. *Compos. B. Eng.* **2018**, *143*, 172−196.

(30) Román-Manso, B.; Weeks, R.; Truby, R.; Lewis, J. Embedded 3D Printing of Architected Ceramics Via Microwave-Activated Polymerization. *Adv. Mater.* **2023**, *35*, 2209270−2209279.

(31) Estakhrianhaghighi, E.; Mirabolghasemi, A.; Zhang, Y.; Lessard, L.; Akbarzadeh, A. 3D-Printed Wood-Fiber Reinforced Architected Cellular Composites. *Adv. Eng. Mater.* **2020**, *22* (11), 2000565−2000578.

(32) Liu, B.; Liu, S.; Devaraj, V.; Yin, Y.; Zhang, Y.; Ai, J.; Han, Y.; Feng, J. Metal 3D Nanoprinting with Coupled Fields. *Nat. Commun.* **2023**, *14* (1), 4920−4930.

(33) Guo, X.; Huang, H.; Zhu, M.; Hariharan, K.; Chien, S.; Huynh, N.; Hwang, J.; Windl, W.; Taylor, C.; Schindelholz, E.; Frankel, G. Interstitial Elements Created Via Metal 3D Printing. *Mater. Today* **2023**, *66*, 92−104.

(34) Xin, A.; Yu, K.; Zhang, R.; Ruan, B.; McGaughey, A. L.; Feng, Z.; Lee, K.; Chen, Y.; Childress, A.; Wang, Q. Bone-Inspired Healing of 3D-Printed Porous Ceramics. *Mater. Horizons* **2020**, *7* (8), 2130−2140.

(35) Li, B.; Xue, Z.; Jiang, B.; Feng, T.; Zhang, L.; Wang, X.; He, J. 3D Printing of Infrared Transparent Ceramics Via Material Extrusion. *Addit. Manuf.* **2023**, *61*, 103364−103373.

(36) Yuk, H.; Lu, B.; Lin, S.; Qu, K.; Xu, J.; Luo, J.; Zhao, X. 3D Printing of Conducting Polymers. *Nat. Commun.* **2020**, *11* (1), 1604−1611.

(37) Zhou, L.; Fu, J.; He, Y. A Review of 3D Printing Technologies for Soft Polymer Materials. *Adv. Funct. Mater.* **2020**, *30* (28), 202000187−202000224.

(38) Wangpraseurt, D.; You, S.; Azam, F.; Jacucci, G.; Gaidarenko, O.; Hildebrand, M.; Kühl, M.; Smith, A. G.; Davey, M. P.; Smith, A.; Deheyn, D. D.; Chen, S.; Vignolini, S. Bionic 3D Printed Corals. *Nat. Commun.* **2020**, *11* (1), 1748−1755.

(39) Rahmani Dabbagh, S.; Rezapour Sarabi, M.; Birtek, M. T.; Mustafaoglu, N.; Zhang, Y. S.; Tasoglu, S. 3D Bioprinted Organ-on-Chips. *Aggregate* **2022**, *4* (1), 197−222.

(40) Muñoz, J.; Redondo, E.; Pumera, M. Chiral 3D-Printed Bioelectrodes. *Adv. Funct. Mater.* **2021**, *31* (16), 2010608−2010616.

(41) Blachowicz, T.; Ehrmann, G.; Ehrmann, A. Metal Additive Manufacturing for Satellites and Rockets. *Appl. Sci.* **2021**, *11* (24), 12036−12050.

(42) Donaldson, L. Simulating Martian Dust for 3D Printing in Space. *Mater. Today* **2022**, *60*, 2−2.

(43) Witze, A. NASA to Send 3D Printer into Space. *Nature* **2014**, *513*, 156.

(44) Rezapour Sarabi, M.; Yetisen, A. K.; Tasoglu, S. Bioprinting in Microgravity. *ACS Biomater. Sci. Eng.* **2023**, *9* (6), 3074−3083.

(45) Luo, J.; Wang, Z.; Xu, L.; Wang, A. C.; Han, K.; Jiang, T.; Lai, Q.; Bai, Y.; Tang, W.; Fan, F. R.; Wang, Z. L. Flexible and Durable Wood-Based Triboelectric Nanogenerators for Self-Powered Sensing in Athletic Big Data Analytics. *Nat. Commun.* **2019**, *10* (1), 5147−5155.

(46) Jiang, Y.; Dong, K.; Li, X.; An, J.; Wu, D.; Peng, X.; Yi, J.; Ning, C.; Cheng, R.; Yu, P.; Wang, Z. L. Stretchable, Washable, and Ultrathin Triboelectric Nanogenerators as Skin-Like Highly Sensitive Self-Powered Haptic Sensors. *Adv. Funct. Mater.* **2020**, *31* (1), 2005584−2005592.

(47) Wang, Y.; Wu, H.; Xu, L.; Zhang, H.; Yang, Y.; Wang, Z. L. Hierarchically Patterned Self-Powered Sensors for Multifunctional Tactile Sensing. *Sci. Adv.* **2020**, *6*, 9083−9091.

(48) Kim, S.; Park, S.; Park, H.; Park, D.; Jeong, Y.; Kim, D. Highly Sensitive and Multimodal All-Carbon Skin Sensors Capable of Simultaneously Detecting Tactile and Biological Stimuli. *Adv. Mater.* **2015**, *27* (28), 4178−4185.

(49) Lu, D.; Liu, T.; Meng, X.; Luo, B.; Yuan, J.; Liu, Y.; Zhang, S.; Cai, C.; Gao, C.; Wang, J.; Wang, S.; Nie, S. Wearable Triboelectric Visual Sensors for Tactile Perception. *Adv. Mater.* **2023**, *35* (7), 2209117−2209126.

(50) Pu, X.; Guo, H.; Chen, J.; Wang, X.; Xi, Y.; Hu, C.; Wang, Z. L. Eye Motion Triggered Self-Powered Mechnosensational Communication System Using Triboelectric Nanogenerator. *Sci. Adv.* **2017**, *3*, 1700694−1700700.

(51) Tao, X.; Li, S.; Shi, Y.; Wang, X.; Tian, J.; Liu, Z.; Yang, P.; Chen, X.; Wang, Z. L. Triboelectric Polymer with High Thermal Charge Stability for Harvesting Energy from 200 °C Flowing Air. *Adv. Funct. Mater.* **2021**, *31* (49), 2106082−2106090.

(52) Feng, L.; Xu, S.; Sun, T.; Zhang, C.; Feng, J.; Yao, L.; Ge, J. Fire/Acid/Alkali-Resistant Aramid/Carbon Nanofiber Triboelectric Nanogenerator for Self-Powered Biomotion and Risk Perception in Fire and Chemical Environments. *Adv. Fiber Mater.* **2023**, *5* (4), 1478−1492.

(53) Xu, C.; Wang, A. C.; Zou, H.; Zhang, B.; Zhang, C.; Zi, Y.; Pan, L.; Wang, P.; Feng, P.; Lin, Z.; Wang, Z. L.; et al. Raising the Working Temperature of a Triboelectric Nanogenerator by Quenching Down Electron Thermionic Emission in Contact-Electrification. *Adv. Mater.* **2018**, *30* (38), 1803968−1803977.

(54) Xing, F.; Ou, Z.; Gao, X.; Chen, B.; Wang, Z. L. Harvesting Electrical Energy from High Temperature Environment by Aerogel Nano-Covered Triboelectric Yarns. *Adv. Funct. Mater.* **2022**, *32* (49), 2205275−2205285.

(55) Zhang, D.; Shi, J.; Wang, Z. L.; Tang, W. Probing Polymer Contact Electrification by Gamma-Ray Radiation. *Front. Mater.* **2022**, *9*, 878885−878891.

(56) Deng, Z.; Li, D.; Qi, P.; Shao, W.; Chen, T.; Song, X.; Kang, Y. Effects of Curvature Radius on Flexible Eddy Current Array Sensors for the Curved Surface of Metal Components. *Front. Phys.* **2022**, *10*, 988009−988021.

(57) Murty, M. V. R. K.; Shukla, R. P. Measurement of Long Radius of Curvature. *Opt. Eng.* **1983**, *22* (2), 231−235.